RESEARCH ARTICLE
PLANETARY SCIENCES

Earth and Planetary Physics
4: 396–402, 2020
doi: 10.26464/epp2020036

Observation of CO_2^{++} dication in the dayside Martian upper atmosphere

Hao Gu[1], Jun Cui[2,3,4*], DanDan Niu[1], LongKang Dai[2], JianPing Huang[2], XiaoShu Wu[3,4], YongQiang Hao[5], and Yong Wei[6,7]

[1]State Key Laboratory of Lunar and Planetary Sciences, Macau University of Science and Technology, Macau 999078, China;

[2]School of Atmospheric Sciences, Sun Yat-Sen University, Zhuhai Guangdong 519082, China;

[3]Key Laboratory of Lunar and Deep Space Exploration, Chinese Academy of Sciences, Beijing 100101, China;

[4]Chinese Academy of Sciences Center for Excellence in Comparative Planetology, Hefei 230026, China;

[5]School of Earth and Space Sciences, Beijing University, Beijing 100871, China;

[6]Institute of Geology and Geophysics, Chinese Academy of Sciences, Beijing 100029, China;

[7]School of Earth and Planetary Sciences, University of Chinese Academy of Sciences, Beijing 100049, China

Key Points:

- CO_2^{++} dication is detected in the Martian ionosphere for the first time
- Simplified photochemical model calculations are carried out and potential reasons for the data-model disagreement are discussed
- The CO_2^{++} abundance in the dayside Martian upper atmosphere is more sensitive to solar irradiance at short wavelengths than the CO_2^+ abundance

Citation: Gu, H., Cui, J., Niu, D. D., Dai, L. K., Huang, J. P., Wu, X. S., Hao, Y. Q., and Wei, Y. (2020). Observation of CO_2^{++} dication in the dayside Martian upper atmosphere. *Earth Planet. Phys.*, *4*(4), 396–402. http://doi.org/10.26464/epp2020036

Abstract: Doubly charged positive ions (dications) are an important component of planetary ionospheres because of the large energy required for their formation. Observations of these ions are exceptionally difficult due to their low abundances; until now, only atomic dications have been detected. The Neutral Gas and Ion Mass Spectrometer (NGIMS) measurements made on board the recent Mars Atmosphere and Volatile Evolution mission provide the first opportunity for decisive detection of molecular dications, CO_2^{++} in this case, in a planetary upper atmosphere. The NGIMS data reveal a dayside averaged CO_2^{++} distribution declining steadily from 5.6 cm^{-3} at 160 km to below 1 cm^{-3} above 200 km. The dominant CO_2^{++} production mechanisms are double photoionization of CO_2 below 190 km and single photoionization of CO_2^+ at higher altitudes; CO_2^{++} destruction is dominated by natural dissociation, but reactions with atmospheric CO_2 and O become important below 160 km. Simplified photochemical model calculations are carried out and reasonably reproduce the data at low altitudes within a factor of 2 but underestimate the data at high altitudes by a factor of 4. Finally, we report a much stronger solar control of the CO_2^{++} density than of the CO_2^+ density .

Keywords: MAVEN; Martian ionosphere; dication

1. Introduction

Despite their low abundances, the study of doubly charged positive ions (dications) has attracted considerable interest over the past few decades, as science has sought a more complete understanding of ionospheric composition on various Solar System bodies (Thissen et al., 2011). The large amounts of input energy required for their formation makes these ions particularly interesting, as does the observation that field-aligned transport of doubly charged ions is exceptionally efficient because they feel an ambipolar electric field force twice as great as the force exerted on singly charged positive ions (monocations). It has also been proposed that the dissociative recombination (DR) of molecular dications makes a non-negligible contribution to atmospheric escape (Lilensten et al., 2013).

The detection of dications in planetary upper atmospheres is difficult (Thissen et al., 2011). O^{++} and S^{++} ions were the first to be measured, O^{++} being detected first in the topside terrestrial ionosphere by the mass spectrometer on board Explorer 31 (Hoffman, 1967); since then, numerous satellite experiments have been made, providing mass spectrometric measurements of O^{++} in the ionospheres of the Earth (Taylor, 1973; Hoffman et al., 1974; Breig et al., 1977, 1982), Venus (Taylor et al., 1980; Ghosh et al., 1995), and Mars (Benna et al., 2015; Gu H et al., 2020). The Galileo plasma analyzers identified O^{++} and S^{++} in Io's ionosphere (Frank et al., 1996; Frank and Paterson, 2001). As observations increased, sever-

Correspondence to: J. Cui, cuijun7@mail.sysu.edu.cn
Received 28 MAR 2020; Accepted 15 APR 2020.
Accepted article online 04 JUN 2020.

al theoretical models predicted O^{++} densities in the upper atmospheres of the Earth (e.g., Breig et al., 1977, 1982) and Venus (e.g., Fox and Victor, 1981).

Despite these efforts, ionospheric molecular dications, such as N_2^{++}, O_2^{++} and CO_2^{++}, have remained undetected until recently, though their presence in the ionosphere of Earth has been predicted for many decades (e.g., Simon et al., 2005) and more recently in that of Mars (e.g., Witasse et al., 2002, 2003), of Titan (e.g., Lilensten et al., 2005), and of Venus (e.g., Gronoff et al., 2007).

In recent years, significant progress has been made to improve the resolution and sensitivity of mass spectrometers. Since the successful launch of the Mars Atmosphere and Volatile Evolution (MAVEN) spacecraft in October 2014 (Jakosky et al., 2015), its Neutral Gas and Ion Mass Spectrometer (NGIMS) has been providing extensive measurements of the Martian ionospheric composition at altitudes from 120 km to 500 km (Mahaffy et al., 2015). We show here that the NGIMS data offer the first opportunity of observing dications, CO_2^{++} in this case, in a planetary ionosphere (Section 2). Simplified model calculations are made to identify its dominant production and destruction processes (Section 3). Potential reasons for disagreement between the data and our model are discussed (Section 4). We also compare CO_2^{++} observations under low and high solar activities (Section 5).

2. Observations of CO_2^{++} Dication

This study relies mainly on ion density data accumulated by the MAVEN NGIMS over three years and a half, up to May 2018. The NGIMS is a high-resolution mass spectrometer with a mass range of 2–150 Da and a mass resolution of 1 Da (Mahaffy et al., 2015). The background level is channel dependent and is typically below 0.01 cm^{-3} (Benna et al., 2015). In this study, the mean count rate in channel $M/Z = 22$ above 300 km, which becomes independent of altitude, is treated as the background level, and is subtracted to obtain two CO_2^{++} density profiles during each orbit, one for inbound and the other one for outbound. The contribution from other ion species such as $^{22}Ne^{++}$ is too tiny to be relevant (Thissen et al., 2011). The NGIMS resolution does not allow reliable detection of some other important dications, such as O_2^{++} and N_2^{++}/CO^{++}, which have the same mass-to-charge ratios as O^+ and N^+, respectively.

During the nominal mission phase, the typical MAVEN periapsis is at ~160 km. To ensure near identical samplings at different altitudes, we show in Figure 1 the dayside averaged CO_2^{++} distribution from 160 km up to 220 km obtained from a total of 831 orbits with periapsis solar zenith angle (SZA) below 85°. The horizontal error bars represent the standard deviations of the CO_2^{++} density measurements within predefined altitude bins with a common width of 5 km. The NGIMS-derived CO_2^{++} density declines steadily with increasing altitude, from 5.6±1.5 cm^{-3} at 160 km to 0.7± 0.3 cm^{-3} at 220 km.

For comparison, the model predictions of Witasse et al. (2003) are superimposed in Figure 1, with the dashed and dash-dotted lines representing the CO_2^{++} profiles appropriate for Viking 1 (V1) and for Mariner 6 (M6) conditions: for V1, the heliocentric distance, SZA, and 10.7 cm solar radio index at the Earth are 1.61 AU, 44°, and 69 SFU (solar flux unit, 10^{-22} m^{-2}·Hz^{-1}); for M6 the respective values are 1.43 AU, 57°, and 166 SFU. Witasse et al.'s calculations predicted a distinctive layer structure peaking at 145 km with different peak densities of 1.4 cm^{-3} (V1) and 4.5 cm^{-3} (M6). In principle, the predicted CO_2^{++} peak could be compared with NGIMS data from two dayside Deep Dip campaigns on 17–22 April 2015 and on 16–23 October 2017, during which the periapsis was lowered to 120–130 km (Stone et al., 2018), but the DD sample is too limited to allow an unambiguous identification of the peak. For this reason, throughout the rest of this paper we focus on the CO_2^{++} distribution above 160 km.

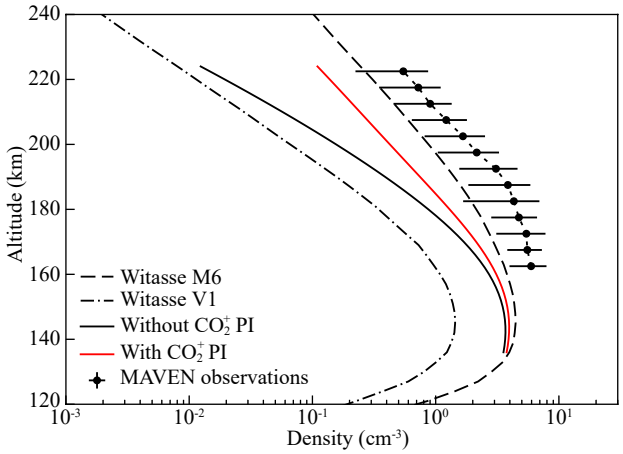

Figure 1. The dayside averaged CO_2^{++} density profile in the Martian upper atmosphere over the altitude range of 160–220 km based on the MAVEN NGIMS measurements, along with standard deviations within the predefined altitude bins. Model profiles from our calculations are superimposed, either with or without CO_2^{++} production from single photoionization of CO_2^+. For comparison, the model predictions of Witasse et al. (2003) appropriate for Viking 1 (V1) and Mariner 6 (M6) conditions are also indicated.

Above the peak, Figure 1 indicates that the observed trend for M6 is consistent with the model prediction, despite that the measured density is on average 50% higher than the predicted density. The V1 model profile is clearly different from observations in both magnitude and trend; at 160 km the measured density is higher by a factor of four than the predicted density and the data-model disagreement is exacerbated with increasing altitude.

A comparison of V6 and M1 model results suggests that the CO_2^{++} distribution in the Martian ionosphere depends critically on the solar illumination condition and the background atmosphere. For a more rigorous interpretation of the NGIMS CO_2^{++} data, it is necessary to repeat the calculations using appropriate model inputs, which is the subject of the next section.

3. A Simplified Photochemical Model of CO_2^{++}

According to laboratory measurements, the natural lifetime of the ground state of CO_2^{++}, denoted as $X^3\Sigma_g^-$, is ~ 4 s before it dissociates to two singly charged fragments (Mathur et al., 1995), while the natural lifetimes of the two excited states, denoted as $A^1\Delta_g$ and $B^1\Sigma_g^+$, are several microseconds (Slattery et al., 2005). Hence

we consider only the ground state CO_2^{++} in our calculations.

Following Witasse et al. (2002, 2003), we assume that CO_2^{++} is produced by the double photoionization (PI) and electron impact ionization (EI) of CO_2, and destroyed via three chemical channels — reactions with CO_2 and DR, and natural dissociation. The reaction of CO_2^{++} with atomic O is also taken into account following Gronoff et al. (2007). Under the condition of photochemical equilibrium (PCE), the CO_2^{++} density, denoted as $n_{CO_2^{2+}}$, is favorably computed from Equation (1) of Witasse et al. (2003), written as

$$n_{CO_2^{2+}} = \frac{P_{CO_2}^{PI} + P_{CO_2}^{EI}}{n_e k_{dr} + n_{CO_2} k_{CO_2} + n_O k_O + \tau_n^{-1}},$$

$P_{CO_2}^{PI}$ is the ion production rate via double PI; $P_{CO_2}^{EI}$ is the ion production rate via double EI; n_e is the thermal electron density; n_{CO_2} is the CO_2 number density; n_O is the O number density; k_{dr} is the DR coefficient; k_{CO_2} is the rate coefficient for the reaction between CO_2^{++} and CO_2; k_O is the rate coefficient for the reaction between CO_2^{++} and O; τ_n is the CO_2^{++} natural lifetime. The relevant rate coefficients are provided in Table 1 for reference.

Table 1. The chemical destruction channels of CO_2^{++} and the respective rate coefficients. (Here T_e and T_n are the electron and neutral temperatures).

Reaction	Rate coefficient ($cm^3 \cdot s^{-1}$)	Reference
$CO_2^{++}+e$	$k_{dr}=6.2\times10^{-7}\ (300/T_e)^{1/2}$	Seiersen et al. (2003)
$CO_2^{++}+CO_2$	$k_{CO_2}=2.1\times10^{-10}\ (T_n/300)^{1/2}$	Franceschi et al. (2003)
$CO_2^{++}+O$	$k_O=2.0\times10^{-9}$	Gronoff et al. (2007)

To improve data-model comparison, the model inputs are adapted from realistic measurements made by several instruments on board MAVEN: (1) The solar Extreme Ultraviolet (EUV) and X-ray flux is based on the level 3 solar spectral model at Mars, constructed from the Flare Irradiance Spectral Model — Mars (Thiemann et al., 2017) and calibrated with Extreme Ultraviolet Monitor (EUVM) band irradiance data (Eparvier et al., 2015); (2) The energetic electron flux from 3 eV to 4.6 keV is taken from the omnidirectional intensity data accumulated by the Solar Wind Electron Analyzer (Mitchell et al., 2016); (3) The neutral densities are obtained from NGIMS level 2 data in the Closed Source Neutral mode (Mahaffy et al., 2015); (4) The electron densities and temperatures are available from the current-voltage characteristics measured by the Langmuir Probe and Waves (LPW) (Andersson et al., 2015); (5) The ion temperatures are based on the moment computation of the O_2^+ energy distribution from Suprathermal and Thermal Ion Composition (STATIC) measurements (McFadden et al., 2015). Later in this section the ion temperatures are used to parameterize ion diffusion.

In Figures 2a and 2b, we show the altitude profiles of various parameters used for calculating the CO_2^{++} production and destruction rates, based on MAVEN data accumulated during the same period of CO_2^{++} observations (see Figure 1). To minimize possible contamination by heterogeneous chemistry on the NGIMS antechamber walls (Stone et al., 2018), only inbound data are used. The displayed neutral density profiles represent logarithmic fittings to the dayside averaged NGIMS data. The electron density profile represents the best-fit to the dayside averaged LPW data with the revised Chapman model of Cui J et al. (2015). The neutral temperature profiles from individual orbits are constructed by downward integrating the CO_2 density profiles, assuming hydrostatic balance (Cui J et al., 2018), from which the dayside averaged temperature profile is computed and fitted polynomially, as displayed. The MAVEN-based averaged ion and electron temperatures, given by the dashed lines in Figure 2b, are empirically modeled using the functional form of Ergun et al. (2015). It is well known that the LPW electron temperatures at relatively low altitudes are seriously overestimated due to surface resistance or capacitance on the LPW instrument sensor (Peterson et al., 2018). To correct for this effect, we derive a modified electron temperature profile using the same functional form but with the lower boundary temperature manually fixed to be close to the neutral temperature. To maintain the expected strong coupling between all constituents (Matta et al., 2014), a similar modification is applied also to the ion temperatures. Our calculations displayed in Figure 2 are based on the modified electron and ion temperatures, as given by the solid lines in panel (b).

The dayside averaged CO_2^{++} production rates via the double PI and EI of CO_2 are provided in Figure 2c, showing that the latter is only 10% of the former. These production rates are computed with the aid of cross section data compiled by Masuoka (1994) and Itikawa (2002). The constancy of the EI–to–PI ratio is consistent with the optically thin (at EUV/X-ray) nature of the regions considered here. In Figure 2d, we show further the chemical destruction timescales of CO_2^{++} for different channels, revealing that natural dissociation dominates at all altitudes except near the lower boundary, where the reaction with CO_2 becomes important. Also, according to our calculations, the reaction with O, which was not considered by Witasse et al. (2002, 2003), cannot be ignored at low altitudes. In addition, DR makes a minor contribution to CO_2^{++} destruction at all altitudes. The last fact implies that any uncertainty in correcting for the low altitude LPW temperatures should not be crucial.

The dayside averaged CO_2^{++} density profile predicted by assuming PCE is given by the black solid line in Figure 1. When compared to NGIMS observations, the model underestimates the CO_2^{++} densities by a factor of 2 at 160 km and by a factor of 35 at 220 km. In the following section we address a number of considerations that may explain disagreement between the model and the empirical data.

4. Potential Sources of Data-Model Disagreement

Various rate coefficients of CO_2^{++} destruction have channel-specific uncertainties of 20%–60% (Franceschi et al., 2003; Seiersen et al., 2003; Gronoff et al., 2007), and the PI and EI cross sections have uncertainties of 6%–30% (Masuoka, 1994). Above the CO_2 double ionization threshold, the uncertainty in the solar EUV/X-ray flux is 20% (Thiemann et al., 2017). In addition, Mahaffy et al. (2015) reported systematic uncertainties in neutral and ion densities to be 20% and 25%, respectively, which cannot be removed by averaging over many orbits. The above uncertainties can be combined to estimate the uncertainty in the predicted CO_2^{++} density,

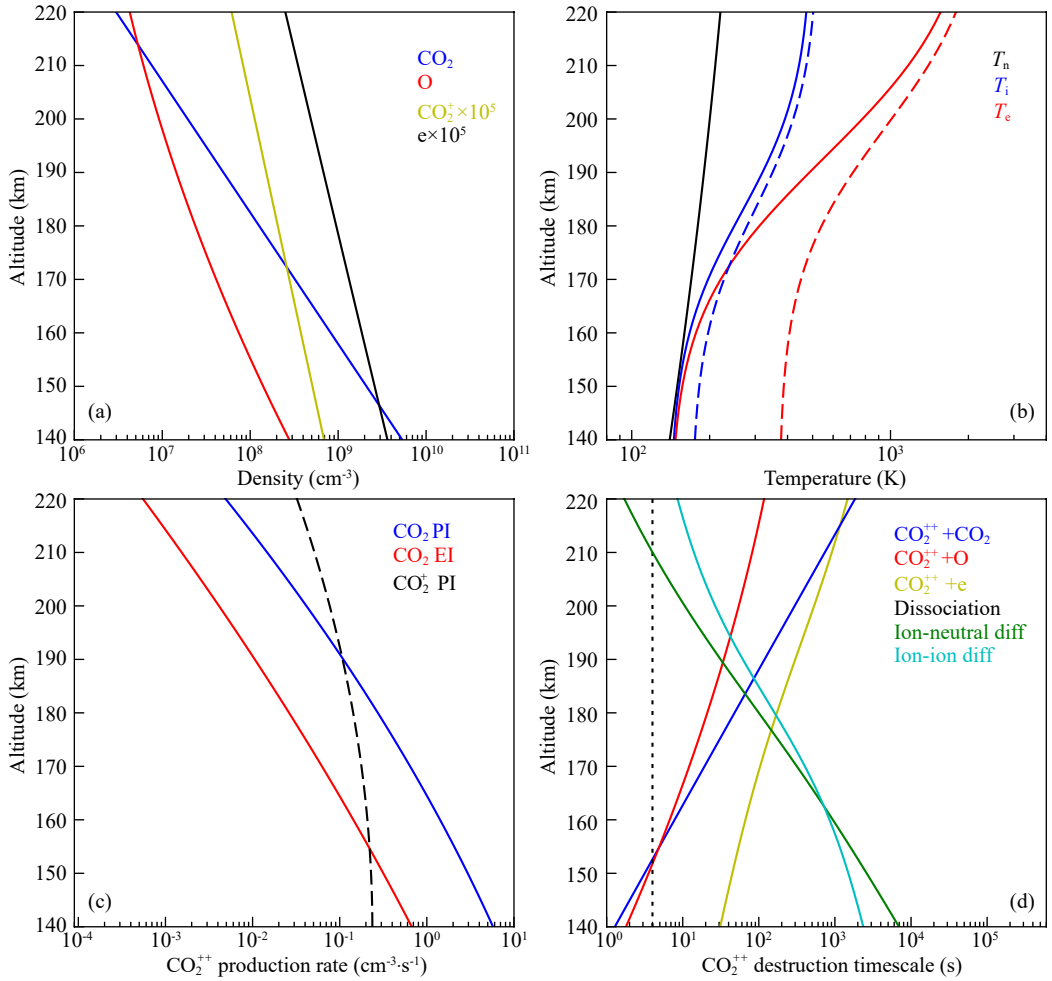

Figure 2. MAVEN-based altitude profiles of various parameters in the dayside averaged sense, including CO_2, O, CO_2^+, and electron densities in panel (a), neutral, ion, and electron temperatures in panel (b), CO_2^{++} production rates via the double PI and EI of CO_2, as well as the single PI of CO_2^+ in panel (c), and in panel (d) various CO_2^{++} destruction timescales as indicated in the figure legend, along with the ion–neutral (CO_2^{++}–CO_2) and ion–ion (CO_2^{++}–O_2^+) diffusion timescales. In panel (b), the solid and dashed lines represent the empirical fittings to direct MAVEN measurements and the modified temperature profiles, respectively (see text for details).

depending on the dominant production and destruction channels at any given altitude. Specifically, the uncertainty near the lower boundary is ~40%, indicating that the predicted density deviates from the observed density by no more than 3σ. At high altitudes, however, it is clear that the combined experimental uncertainty is insufficient to explain the model's serious underestimates.

The model calculations presented so far are made assuming PCE, but at high altitudes diffusion is likely more important than photochemistry (e.g. Fox, 2009). The CO_2^{++} diffusion timescales are presented in Figure 2d. The figure indicates that diffusion becomes important only above 200 km. To evaluate CO_2^{++} diffusion properly, ion–neutral and ion–ion collisions should both be considered (Matta et al., 2013). Note that the respective collision frequencies should be enhanced by a factor of $\sqrt{2}$ (ion–neutral) or 2 (ion–ion) for CO_2^{++} dication relative to CO_2^+ monocation (Schunk and Nagy, 2009). In addition, the effect of diffusion is manifest as a bulk CO_2^{++} outflow (e.g. Wu XS et al., 2019), which reduces topside CO_2^{++} densities and causes an even larger discrepancy between model results and observations.

The above discussions imply that extra sources of CO_2^{++} are required. One candidate is the single photoionization of CO_2^{++}, which was not considered by Witasse et al. (2002, 2003). Laboratory measurements of the relevant cross section cover the energy range of 23–26 eV (Bizau et al., 2012), which is too narrow to be directly applicable to our calculations. Here for illustrative purposes, we assume that the ratio of the single PI frequency of CO_2^+ to the double PI frequency of CO_2 is equal to the respective O^+ to O ratio. The altitude profiles of the CO_2^+ PI rate and CO_2^{++} density thus obtained are displayed in Figures 2c and 1, respectively. Our calculations indicate that this extra channel is important at high altitudes. Near the upper boundary, it increases the predicted CO_2^{++} density under PCE by a factor of 9 and hence reduces the model difference from the observed density to a factor of 4. Although the effect is expected to be small, inclusion of the single ionization of CO_2^+ by photoelectrons should improve further the data-model agreement.

5. Solar Control of CO_2^{++} Dication

NGIMS measurements exhibit a clear solar cycle variation in the CO_2^{++} distribution. This is displayed in Figure 3, comparing the dayside averaged CO_2^{++} profiles under low and high solar activity conditions (defined as an integrated solar EUV/X-ray energy flux of less than or greater than 1.2 erg·cm^{-2}·s^{-1}, based on the EUVM solar spectral model up to 90 nm). These two cases include 464 and 367 orbits, respectively. Figure 3 reveals a remarkable difference between the two cases, indicating a strong influence of solar EUV/X-ray radiation on CO_2^{++} abundance in the dayside Martian upper atmosphere. According to Section 3, the density difference is a function of the differences in both the solar irradiance and background atmosphere, except near the lower boundary where the difference in the background atmosphere drops out because there the rates of production and of destruction of CO_2^{++} are both proportional to neutral density.

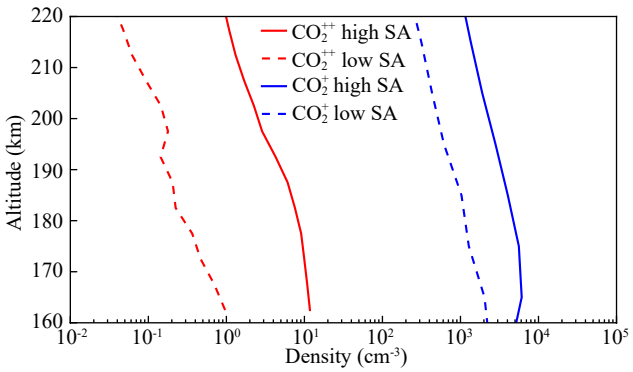

Figure 3. A comparison of the dayside averaged CO_2^{++} and CO_2^{+} density profiles between high and low solar activity conditions, defined as integrated solar EUV/X-ray energy flux at Mars up to 90 nm of less than or greater than 1.2 erg·cm^{-2}·s^{-1}. The two cases contain 464 and 367 orbits, respectively.

It is also instructive to compare monocations and dications in terms of their different responses to solar inputs. Figure 3 presents CO_2^{++} density profiles under high and low solar activity conditions, indicating that from low to high solar activities, the CO_2^{+} monocation density increases on average by a factor of 4, but the CO_2^{++} dication density increases by a factor of 25. Without showing the details, we mention that a similar difference is also seen between O^{++} and O^{+} (see also Gu H et al., 2020). These observations clearly demonstrate that the abundances of dications are more sensitive to solar irradiance at short wavelengths than are the abundances of monocations.

A more pronounced difference in CO_2^{++} density between different solar inputs is related to an enhanced variability in the solar irradiance at short wavelengths combined with a larger energy required for CO_2^{++} formation (above 37.6 eV) as compared to CO_2^{+} formation (above 13.8 eV) (Masuoka, 1994). Meanwhile, the dominant CO_2^{+} destruction channel is its reaction with atmospheric O, whose abundance is enhanced under high solar activities because of enhanced photolysis of CO_2 and CO (e.g., Withers et al., 2015). Hence enhanced CO_2^{+} production under high solar activities is partially counterbalanced by enhanced CO_2^{+} destruction. This is to be distinguished from CO_2^{++}, which is destroyed mainly via natural dissociation at a constant frequency, independent of solar inputs (Mathur et al., 1995). The above distinction is responsible for the stronger solar control of CO_2^{++} than of CO_2^{+}.

6. Concluding Remarks

The study of dications in planetary upper atmospheres has attracted extensive research interest over the past few decades. Historically, observations have been made only of atomic dications such as O^{++} and S^{++} (Simon et al., 2005; Thissen et al., 2011, and references therein). The NGIMS instrument on board MAVEN has been providing extensive measurements of the ionospheric composition on Mars (Benna et al., 2015), allowing the first ever detection of molecular dications, CO_2^{++} in this case, in a planetary upper atmosphere.

The NGIMS-measured CO_2^{++} density decreases steadily with altitude from 5.6 cm^{-3} at 160 km to below 1 cm^{-3} above 200 km. Using MAVEN-based model inputs, we calculate the CO_2^{++} density profile under PCE. Our calculations suggest that the dominant CO_2^{++} production channel is the double PI of CO_2 below 190 km and the single PI of CO_2^{+} at higher altitudes; CO_2^{++} is destroyed primarily via natural dissociation over the entire altitude range of interest but the contributions from its reactions with CO_2 and O are important near the lower boundary. Meanwhile, ion diffusion becomes non-negligible above 200 km. The CO_2^{++} density predicted by our nominal model is lower than the NGIMS-measured density by a factor of 2 at 160 km and by a factor of 4 at 220 km. Considering the combined experimental uncertainty of at least 40%, we conclude that our model reasonably reproduces the data at low altitudes but modestly underestimates the data at high altitudes. A better data-model agreement could possibly be achieved once improved knowledge of the relevant cross sections and reaction coefficients becomes available (e.g. Bizau et al., 2012).

Finally, our analysis reveals the expected strong solar control of the CO_2^{++} distribution in the dayside Martian upper atmosphere, manifest as a factor of 25 density enhancement under high solar activity relative to low solar activity. Such a density enhancement is much greater (by a factor of 4 four) than that observed for CO_2^{+}, indicating that the abundances of dications are more sensitive to the solar irradiance at short wavelengths than are the abundances of monocations. This is partly due to the larger energy required for CO_2^{++} formation and partly due to enhanced CO_2^{+} destruction in response to enhanced thermospheric O abundances at higher levels of solar activitiy.

Acknowledgments

This work is supported by the B-type Strategic Priority Program No. XDB41000000 funded by the Chinese Academy of Sciences, and the pre-research projects on Civil Aerospace Technologies No. D020105 and D020103 funded by China's National Space Administration. The authors also acknowledge support from the National Science Foundation of China through grants 41525015 and 41774186 to JC, 41904154 to WXS, and 41525016 to YW. The multi-instrument MAVEN data set used in this work is publicly available at the MAVEN Science Data Center (http://lasp.colorado.edu/maven/sdc/public/).

References

Andersson, L., Ergun, R. E., Delory, G. T., Eriksson, A., Westfall, J., Reed, H., McCauly, J., Summers, D., and Meyers, D. (2015). The Langmuir Probe and Waves (LPW) instrument for MAVEN. *Space Sci. Rev.*, *195*(1–4), 173–198. https://doi.org/10.1007/s11214-015-0194-3

Benna, M., Mahaffy, P. R., Grebowsky, J. M., Fox, J. L., Yelle, R. V., and Jakosky, B. M. (2015). First measurements of composition and dynamics of the Martian ionosphere by MAVEN's Neutral Gas and Ion Mass Spectrometer. *Geophys. Res. Lett.*, *42*(21), 8958–8965. https://doi.org/10.1002/2015GL066146

Bizau, J. M., Cubaynes, D., Shorman, M. M. A., Guilbaud, S., Blancard, C., Lemaire, J., Thissen, R., Giuliani, A., Nicolas, C., and Milosavljević, A. R. (2012). Photoionization of atomic and molecular positively charged ions. *J. Phys. Conf. Ser.*, *399*, 012002. https://doi.org/10.1088/1742-6596/399/1/012002

Breig, E. L., Torr, M. R., Torr, D. G., Hanson, W. B., Hoffman, J. H., Walker, J. G. G., and Nier, A. O. (1977). Doubly charged atomic oxygen ions in the thermosphere, 1. *Photochemistry. J. Geophys. Res.*, *82*(7), 1008–1012. https://doi.org/10.1029/JA082i007p01008

Breig, E. L., Torr, M. R., and Kayser, D. C. (1982). Observations and photochemistry of O^{++} in the daytime thermosphere. *J. Geophys. Res. Space Phys.*, *87*(A9), 7653–7665. https://doi.org/10.1029/JA087iA09p07653

Cui, J., Galand, M., Zhang, S. J., Vigren, E., and Zou, H. (2015). The electron thermal structure in the dayside Martian ionosphere implied by the MGS radio occultation data. *J. Geophys. Res. Planets*, *120*(2), 278–286. https://doi.org/10.1002/2014JE004726

Cui, J., Yelle, R. V., Zhao, L. L., Stone, S., Jiang, F. Y., Cao, Y. T., Yao, M. J., Koskinen, T. T., and Wei, Y. (2018). Astrophys. *J. Lett.*, *853*(2), L33. https://doi.org/10.3847/2041-8213/aaa89a

Eparvier, F. G., Chamberlin, P. C., Woods, T. N., and Thiemann, E. M. B. (2015). The solar extreme ultraviolet monitor for MAVEN. *Space Sci. Rev.*, *195*(1–4), 293–301. https://doi.org/10.1007/s11214-015-0195-2

Ergun, R. E., Morooka, M. W., Andersson, L. A., Fowler, C. M., Delory, G. T., Andrews, D. J., Eriksson, A. I., McEnulty, T., and Jakosky, B. M. (2015). Dayside electron temperature and density profiles at Mars: First results from the MAVEN Langmuir probe and waves instrument. *Geophys. Res. Lett.*, *42*(21), 8846–8853. https://doi.org/10.1002/2015GL065280

Fox, J. L., and Victor, G. A. (1981). O^{++} in the Venusian ionosphere. *J. Geophys. Res. Space Phys.*, *86*(A4), 2438–2442. https://doi.org/10.1029/JA086iA04p02438

Fox, J. L. (2009). Morphology of the dayside ionosphere of Mars: Implications for ion outflows. *J. Geophys. Res. Planets*, *114*(E12), E12005. https://doi.org/10.1029/2009JE003432

Franceschi, P., Thissen, R., Žabka, J., Roithová, J., Herman, Z., and Dutuit, O. (2003). Internal energy effects in the reactivity of CO_2^{2+} doubly charged molecular ions with CO_2 and CO. *Int. J. Mass Spectrom.*, *228*(2–3), 507–516. https://doi.org/10.1016/S1387-3806(03)00157-X

Frank, L. A., Paterson, W. R., Ackerson, K. L., Vasyliunas, V. M., Coroniti, F. V., and Bolton, S. J. (1996). Plasma observations at Io with the Galileo spacecraft. *Science*, *274*(5286), 394–395. https://doi.org/10.1126/science.274.5286.394

Frank, L. A., and Paterson, W. R. (2001). Survey of thermal ions in the Io plasma torus with the Galileo spacecraft. *J. Geophys. Res. Space Phys.*, *106*(A4), 6131–6149. https://doi.org/10.1029/2000JA000159

Ghosh, S., Mahajan, K. K., Grebowsky, J. M., and Nath, N. (1995). Morphology of O^{++} ions and their maintenance in the nightside Venus ionosphere. *J. Geophys. Res. Space Phys.*, *100*(A12), 23983–23991. https://doi.org/10.1029/95JA01581

Gronoff, G., Lilensten, J., Simon, C., Witasse, O., Thissen, R., Dutuit, O., and Alcaraz, C. (2007). Modelling dications in the diurnal ionosphere of Venus. *Astron. Astrophys.*, *465*(2), 641–645. https://doi.org/10.1051/0004-6361:20065991

Gu, H., Cui, J., He, Z. G., and Zhong, J. H. (2020). A MAVEN investigation of O^{++} in the dayside Martian ionosphere. *Earth Planet. Phys.*, *4*(1), 11–16. https://doi.org/10.26464/epp2020009

Hoffman, J. H. (1967). Composition measurements of the topside ionosphere. *Science*, *155*(3760), 322–324. https://doi.org/10.1126/science.155.3760.322

Hoffman, J. H., Dodson, W. H., Lippincott, C. R., and Hammack, H. D. (1974). Initial ion composition results from the Isis 2 satellite. *J. Geophys. Res.*, *79*(28), 4246–4251. https://doi.org/10.1029/JA079i028p04246

Itikawa, Y. (2002). Cross sections for electron collisions with carbon dioxide. *J. Phys. Chem. Ref. Data*, *31*(3), 749–769. https://doi.org/10.1063/1.1481879

Jakosky, B. M., Lin, R. P., Grebowsky, J. M., Luhmann, J. G., Mitchell, D. F., Beutelschies, G., Priser, T., Acuna, M., Andersson L., … Zurek, R. (2015). The Mars atmosphere and volatile evolution (MAVEN) mission. *Space Sci. Rev.*, *195*(1–4), 3–48. https://doi.org/10.1007/s11214-015-0139-x

Lilensten, J., Witasse, O., Simon, C., Soldi-Lose, H., Dutuit, O., Thissen, R., and Alcaraz, C. (2005). Prediction of a N_2^{++} layer in the upper atmosphere of Titan. *Geophys. Res. Lett.*, *32*(3), L03203. https://doi.org/10.1029/2004GL021432

Lilensten, J., Simon Wedlund, C., Barthélémy, M., Thissen, R., Ehrenreich, D., Gronoff, G., and Witasse, O. (2013). Dications and thermal ions in planetary atmospheric escape. *Icarus*, *222*(1), 169–187. https://doi.org/10.1016/j.icarus.2012.09.034

Mahaffy, P. R., Benna, M., King, T., Harpold, D. N., Arvey, R., Barciniak, M., Bendt, M., Carrigan, D., Errigo, T., … Nolan, J. T. (2015). The neutral gas and ion mass spectrometer on the mars atmosphere and volatile evolution mission. *Space Sci. Rev.*, *195*(1-4), 49–73. https://doi.org/10.1007/s11214-014-0091-1

Masuoka, T. (1994). Single- and double-photoionization cross sections of carbon dioxide (CO_2) and ionic fragmentation of CO_2^+ and CO_2^{2+}. *Phys. Rev. A*, *50*(5), 3886–3894. https://doi.org/10.1103/PhysRevA.50.3886

Mathur, D., Andersen, L. H., Hvelplund, P., Kella, D., and Safvan, C. P. (1995). Long-lived, doubly charged diatomic and triatomic molecular ions. *J. Phys. B At. Mol. Phys.*, *28*(15), 3415–3426. https://doi.org/10.1088/0953-4075/28/15/027

Matta, M., Withers, P., and Mendillo, M. (2013). The composition of Mars' topside ionosphere: Effects of hydrogen. *J. Geophys. Res. Space Phys.*, *118*(5), 2681–2693. https://doi.org/10.1002/jgra.50104

Matta, M., Galand, M., Moore, L., Mendillo, M., and Withers, P. (2014). Numerical simulations of ion and electron temperatures in the ionosphere of Mars: Multiple ions and diurnal variations. *Icarus*, *227*, 78–88. https://doi.org/10.1016/j.icarus.2013.09.006

McFadden, J. P., Kortmann, O., Curtis, D., Dalton, G., Johnson, G., Abiad, R., Sterling, R., Hatch, K., Berg, P., … Jakosky, B. (2015). MAVEN suprathermal and thermal ion compostion (STATIC) instrument. *Space Sci. Rev.*, *195*(1-4), 199–256. https://doi.org/10.1007/s11214-015-0175-6

Mitchell, D. L., Mazelle, C., Sauvaud, J. A., Thocaven, J. J., Rouzaud, J., Fedorov, A., Rouger, P., Toublanc, D., Taylor, E., … Jakosky, B. M. (2016). The MAVEN solar wind electron analyzer. *Space Sci. Rev.*, *200*(1–4), 495–528. https://doi.org/10.1007/s11214-015-0232-1

Peterson, W. K., Fowler, C. M., Andersson, L. A., Thiemann, E. M. B., Jain, S. K., Mayyasi, M., Esman, T. M., Yelle, R., Benna, M., and Espley, J. (2018). Martian electron temperatures in the subsolar region: MAVEN observations compared to a one-dimensional model. *J. Geophys. Res. Space Phys.*, *123*(7), 5960–5973. https://doi.org/10.1029/2018JA025406

Schunk, R. W., and Nagy, A. F. (2009). *Ionospheres: Physics, Plasma Physics, and Chemistry* (2nd ed). New York: Cambridge Univ. Press.

Seiersen, K., Al-Khalili, A., Heber, O., Jensen, M. J., Nielsen, I. B., Pedersen, H. B., Safvan, C. P., and Andersen, L. H. (2003). Dissociative recombination of the cation and dication of CO_2. *Phys. Rev. A*, *68*(2), 022708. https://doi.org/10.1103/PhysRevA.68.022708

Simon, C., Lilensten, J., Dutuit, O., Thissen, R., Witasse, O., Alcaraz, C., and Soldi-Lose, H. (2005). Prediction and modelling of doubly-charged ions in the Earth's upper atmosphere. *Ann. Geophys.*, *23*(3), 781–797. https://doi.org/10.5194/angeo-23-781-2005

Slattery, A. E., Field, T. A., Ahmad, M., Hall, R. I., Lambourne, J., Penent, F., Lablanquie, P., and Eland, J. H. D. (2005). Spectroscopy and metastability of CO_2^{2+} molecular ions. *J. Chem. Phys.*, *122*(8), 084317. https://doi.org/10.1063/1.1850895

Stone, S. W., Yelle, R. V., Benna, M., Elrod, M. K., and Mahaffy, P. R. (2018). Thermal structure of the Martian upper atmosphere from MAVEN NGIMS. *J. Geophys. Res. Planets*, *123*(11), 2842–2867. https://doi.org/10.1029/2018JE005559

Taylor, Jr. H. A. (1973). Parametric description of thermospheric ion

composition results. *J. Geophys. Res.*, *78*(1), 315–319. https://doi.org/10.1029/JA078i001p00315

Taylor, H. A., Brinton, H. C., Wagner, T. C. G., Blackwell, B. H., and Cordier, G. R. (1980). Bennett ion mass spectrometers on the Pioneer Venus Bus and orbiter. *IEEE Trans. Geosci. Remote Sens.*, *GE-18*(1), 44–49. https://doi.org/10.1109/TGRS.1980.350259

Thiemann, E. M. B., Chamberlin, P. C., Eparvier, F. G., Templeman, B., Woods, T. N., Bougher, S. W., and Jakosky, B. M. (2017). The MAVEN EUVM model of solar spectral irradiance variability at Mars: Algorithms and results. *J. Geophys. Res. Space Phys.*, *122*(3), 2748–2767. https://doi.org/10.1002/2016JA023512

Thissen, R., Witasse, O., Dutuit, O., Wedlund, C. S., Gronoff, G., and Lilensten, J. (2011). Doubly-charged ions in the planetary ionospheres: a review. *Phys. Chem. Chem. Phys.*, *13*(41), 18264–18287. https://doi.org/10.1039/C1CP21957J

Witasse, O., Dutuit, O., Lilensten, J., Thissen, R., Zabka, J., Alcaraz, C., Blelly, P. L., Bougher, S. W., Engel, S., … Seiersen, K. (2002). Prediction of a CO_2^{2+} layer in the atmosphere of Mars. *Geophys. Res. Lett.*, *29*(8), 104–1. https://doi.org/10.1029/2002GL014781

Witasse, O., Dutuit, O., Lilensten, J., Thissen, R., Zabka, J., Alcaraz, C., Blelly, P. L., Bougher, S. W., Engel, S., … Seiersen, K. (2003). Correction to "Prediction of a CO_2^{2+} layer in the atmosphere of Mars". *Geophys. Res. Lett.*, *30*(7), 1360. https://doi.org/10.1029/2003GL017007

Withers, P., Vogt, M., Mahaffy, P., Benna, M., Elrod, M., and Jakosky, B. (2015). Changes in the thermosphere and ionosphere of Mars from Viking to MAVEN. *Geophys. Res. Lett.*, *42*(21), 9071–9079. https://doi.org/10.1002/2015GL065985

Wu, X. S., Cui, J., Xu, S. S., Lillis, R. J., Yelle, R. V., Edberg, N. J. T., Vigren, E., Rong, Z. J., Fan, K., … Mitchell, D. L. (2019). The morphology of the topside Martian ionosphere: implications on bulk ion flow. *J. Geophys. Res. Planets*, *124*(3), 734–751. https://doi.org/10.1029/2018JE005895